Value of 1H-Magnetic Resonance Spectroscopy Chemical Shift Imaging (CSI) for Detection of Anaplastic Foci in Diffusely Infiltrating Gliomas with Non-Significant Contrast- Enhancement

Georg Widhalm, Martin Krssak, Georgi Minchev, Adelheid Woehrer, Tatjana Traub-Weidinger, Thomas Czech, Susanne Asenbaum, Christine Marosi, Engelbert Knosp, Johannes A. Hainfellner, et al.

Revision II submitted to *JNNP*, July 2010

Value of ^{1}H-Magnetic Resonance Spectroscopy Chemical Shift Imaging (CSI) for Detection of Anaplastic Foci in Diffusely Infiltrating Gliomas with Non-Significant Contrast-Enhancement

Georg Widhalm, MD[1,2], Martin Krssak, PhD[3], Georgi Minchev, MD[1], Adelheid Wöhrer, MD[2], Tatjana Traub-Weidinger, MD[4], Thomas Czech, MD[1], Susanne Asenbaum, MD[5], Christine Marosi, MD[6], Engelbert Knosp, MD[1], Johannes A. Hainfellner, MD[2], Daniela Prayer, MD[3] and Stefan Wolfsberger, MD[1]

Departments of [1]Neurosurgery, [2]Institute of Neurology, Departments of [3]Radiology, [4]Nuclear Medicine, [5]Neurology and [6]Internal Medicine I of the Medical University Vienna, Austria

Corresponding author

Stefan Wolfsberger, MD

Department of Neurosurgery, Medical University Vienna,

Waehringer Guertel 18-20, 1097 Vienna, Austria

phone +43/1/40400-4565, fax +43/1/40400-4566

e-mail: stefan.wolfsberger@meduniwien.ac.at

Keywords

Diffusely infiltrating gliomas

Chemical shift imaging

Methionine positron emission tomography

Correlation of maxima

Proliferation rate

Word Count- 4093

Abbreviations (in alphabetical order)

2D	Two-dimensional
CE	Contrast-Enhancement
Cho	Choline
Cr	Creatine
CSI	Chemical shift imaging
DIG	Diffusely infiltrating gliomas
FET-PET	^{18}F- fluoroethyl-L-tyrosine PET
MET-PET	^{11}C-methionine-PET
MRI	Magnetic resonance imaging
MRS	Magnetic resonance spectroscopy
NAA	N-acetylaspartate
PET	Positron emission tomography
T/N ratio	Tumor to normal brain ratio
ROI	Region of interest
SUV	Standard uptake value
T	Tesla

ABSTRACT

Objective: In diffusely infiltrating gliomas (DIG), positron emission tomography (PET) imaging is a powerful method for detection of anaplastic foci. Recently, ^{1}H-magnetic resonance spectroscopy chemical shift imaging (CSI) using choline/creatine (Cho/Cr) or choline/N-acetylaspartate (Cho/NAA) ratios has emerged as new non-invasive, widely available alternative. We therefore correlated CSI with ^{11}C-methionine (MET)-PET data in a series of DIG with non-significant contrast-enhancement (CE).

Methods: Thirty-two patients with DIG were examined with single slice CSI on 3 Tesla MRI and MET-PET. Maximum pathologic intratumoral ratios of CSI (=CSI_{max}) and maximum tumor-to-normal-brain PET ratios (=$PET_{max;}$ T/N ratio) were determined. Co-registration of MRI with CSI and PET was performed and the topographic overlap of CSI_{max} and PET_{max} was analyzed. Histologic criteria of anaplasia as well as cell proliferation rate was assessed in tumor samples inside and outside of CSI_{max}.

Results: CSI showed a pathologic ratio in all patients, whereas PET demonstrated a pathologic T/N ratio in 21/32 patients. Topographical correlation of CSI_{max} and PET_{max} revealed a ≥50% overlap in 18/21 and <50% overlap in 3/21 patients, respectively. Cho/Cr_{max} and Cho/NAA_{max} showed a ≥50% overlap in 24/32, a <50% overlap in 8/32 patients. Cell proliferation rate was significantly higher inside than outside the CSI_{max} (13.6% versus 6.9%, *p<0.001*).

Conclusion: Our results indicate that CSI is a promising method for detection of anaplastic foci within DIG with non-significant CE. Intraoperative use of CSI by multimodal neuronavigation may increase the reliability of detection of malignant areas in glioma surgery and therefore optimize allocation of patients to adjuvant treatments.

INTRODUCTION

Standard neuroradiological imaging of diffusely infiltrating gliomas (DIG) by magnetic resonance imaging (MRI) is frequently not able to visualize the most malignant areas within these potentially heterogenous tumors.[1-4] However, intraoperative identification of anaplastic foci is essential, because only representative histology indicates which postoperative therapy is adequate.

In DIG with non-significant contrast-enhancement (CE), positron emission tomography (PET) represents a clinically useful method for the preoperative detection of malignant areas. For this purpose, the metabolic information of amino-acid tracers, e.g. ^{11}C-methionine-PET (MET-PET) or ^{18}F- fluoroethyl-L-tyrosine-PET (FET-PET), is frequently used.[5-10] In case of MET-PET, histological analysis confirmed that voxels with maximum tracer uptake (=PET_{max}) represent the most malignant tumor areas.[8,9,11,12] Therefore, neuronavigation based on MET-PET data co-registered with anatomic images is a powerful tool in glioma surgery:[13,14] In cases of biopsy, the accurate targeting of the most malignant tumor area indicated by PET_{max} is supported; in cases of tumor resection, reliable removal of the most malignant tumor areas is warranted. Further, MET-PET imaging is useful for postoperative follow-up of low-grade gliomas: In these patients, PET facilitates early recognition of tumor progression and recurrence.[9,15] Altogether, MET-PET plays an important role in preoperative planning, intraoperative multimodal neuronavigation and postoperative follow-up of glioma patients.

However, PET exposes the patient to radiation exposure and is only available in highly specialized neurooncological centers. Thus, an alternative diagnostic tool is of interest:

Multivoxel proton magnetic resonance spectroscopy (MRS), termed chemical shift imaging (CSI), has recently emerged as a promising non-invasive metabolic imaging technique. CSI can be performed in the frame of standard MRI with short acquisition time and is thus a widely available investigational tool. Like PET, CSI allows intratumoral detection of most malignant areas by examination of the spatial distribution of metabolites in DIG. Typically, CSI metabolic profile of gliomas includes: Increase of choline (Cho), due to increased cell membrane turnover, a reduction or loss of N-acetyl-L-aspartate (NAA), as a consequence of impairment of neuronal function, a frequently encountered reduction of creatine (Cr), a marker for tissue energy metabolism due to a hypermetabolic state, and the common presence of lipide and lactate due to tissue necrosis and change to anaerobic metabolism.[16-20] For identification of the most malignant intratumoral areas within gliomas, the clinical use of the metabolite ratios Cho/Cr[18,21-28] and Cho/NAA[10,18,21-23,25,26] has been established.

To analyze the ability of this new metabolic imaging technique to detect anaplastic foci in DIG with non-significant CE, we determined the maximum intratumoral ratios of CSI metabolites (=CSI_{max}), performed a topographic correlation of CSI_{max} with MET-PET and assessed histological criteria of anaplasia as well as cell proliferation rate in tumor samples inside and outside of CSI_{max}.

METHODS

The study cohort comprises a consecutive series of 38 patients with DIG with non-significant CE treated at the Department of Neurosurgery of the Medical University of Vienna between July 2007 and November 2009. This study was approved by the ethics committee of the Medical University of Vienna.

All patients underwent MRI, CSI and MET-PET investigations within two weeks before the neurosurgical procedure. After topographic correlation of CSI and MET-PET data, 6/38 patients had to be excluded for the following reasons: In 3 patients, PET_{max} was too close to the skull which did not allow a reliable CSI analysis due to bone artifacts; in 3 further patients, the CSI slice was outside of PET_{max} as CSI examinations were performed without knowledge of MET-PET results. Therefore, 32 patients (16 females, 16 males) remained for further analysis (*table 1*): The median age of our study cohort was 44 years (range 16-66 years). In 21 (66%) patients gross total resection was performed, 6 (19%) patients had partial resection, and 5 (15%) patients underwent stereotactic biopsy. The extent of resection was assessed on T2-weighted MRI performed within 48 hours postoperatively. Tumor localisation was supratentorial in all cases. Newly diagnosed tumors were present in 23 cases and 9 patients with previous surgery for low grade gliomas had suspected tumor recurrence/progression. None of the patients had previously received radio- or chemotherapy.

MET-PET investigations

Patients received 800-850 MBq ^{11}C-methionine after fasting for 4 hours. PET images were then obtained from a dedicated full-ring GE Advance PET scanner (General Electric Medical Systems, Milwaukee, Wisconsin, USA). For detailed description of radiotracer production, data acquisition and reconstruction see.[29]

The scanner produces 35 slices with a slice thickness of 4.25 mm in a field of view of 14.875 cm. The spatial resolution of the scanner in axial direction is 4.0 mm and in tangential direction 3.8 mm. Image reconstruction was done by filtered back projection using a Hanning Filter with a cut-off value of 6.2 mm and a 256x256 matrix.

For the semiquantitative evaluation of tracer accumulation in tumor tissue the standardized uptake value (SUV) and the calculated ratio tumor/contralateral normal tissue (T/N ratio) were used. SUV was defined as radioactive concentration (MBq/g)/injected dose (MBq)*body weight (g). For quantification, a circular region of interest (ROI) was drawn over the tumor lesion with knowledge of tumor localization from structural imaging and clinical data and covering the hottest pixel of the lesion. Afterwards this ROI was mirrored contralaterally to the non-affected hemisphere. Maximal SUVs of these ROIs and T/N ratios were calculated.

PET_{max} definition

To define a threshold for pathologic tracer uptake in PET, a T/N ratio was considered as *normal* below 1.15 or as *non-specific* (1.15 to <1.5). A T/N ratio $\geq$1.5 was regarded as *pathologic*. Areas with highest pathologic T/N ratios, reflecting most intense tracer uptake, were defined as PET_{max}.

MRI/CSI investigations

Our routine MRI protocol for brain tumors consisted of axial fluid-attenuated-inversion-recovery sequences, diffusion-weighted images, axial, coronal T1- and T2-weighted sequences, and contrast-enhanced axial, coronal and sagittal T1-weighted sequences. All gliomas were classified by a neuroradiologist (D.P.) according to the pattern of CE: Only patients with none or unspecific (defined as "patchy" and "faint") CE were included in the study cohort of the initial 38 cases. Patients with unequivocal (defined as "nodular" or "ring-like") CE as a target for tissue sampling were not part of this study.

With the CSI software integrated in our routine clinical 3 Tesla (T) MRI scanner (Tim Trio, Siemens, Erlangen, Germany), single slice (2D) CSI examination could be performed in the course of the same examination as morphologic MRI.

The protocol for CSI consisted of a T2-weighted turbo spin echo sequence and a contrast-enhanced axial T1-weighted gradient echo sequence for navigation purposes. Point-resolved spectroscopy sequence (PRESS; repetition time/effective echo time 1500/135 ms) preceded by chemical shift selective (CHESS) water suppression was used for excitation of rectangular voxel of interest (VOI) selection (4-12 cm in both plane dimensions) excluding skull and subcutaneous tissue contamination. The position of the CSI slice was chosen to cross the largest diameter of the lesion on T2-weighted images. Sequence parameters included 16x16 elliptical weighted phase-encoding steps across a 16x16 cm field of view (FOV), slice thickness of 1 cm, 50% Hamming filter and 3 averages. Application of Hamming filter reduces the effect of "point-spread-function" and affects the volume resolution from nominal cubic volume 1 cm^3 to effective overlapping cylindrical volumes of ~ 1.8 cm^3. The total acquisition time was less than 7 minutes.

Maps of the metabolic ratios Cho/total NAA (=NAA and N-acetylaspartylglutamate) and Cho/Cr were produced using the spectroscopy application within the spectrometer operating system (SyngoMR VB13 and VB15, Siemens, Erlangen, Germany). After zero filling, phasing, filtering (Hanning Filter, 400 ms) of the data, polynomial baseline correction was applied and line fit in the frequency domain was used to obtain Cho, Cr and total NAA signal intensity (area under the peak). Metabolic ratio maps were created within the VOI using the numerical value interpolation as implemented by the manufacturer.

The CSI postprocessing software uses a rainbow-type color lookup-table whereby blue-green-yellow-red correspond to values from zero to maximum (*see figure 1*).

CSI_{max} definition

A threshold of CSI ratio is needed to define pathological areas. Therefore, we tested various ratios in pilot CSI examinations preceding our study: We compared tumor areas with the contralateral tumor-free white matter. Both, for Cho/Cr and Cho/NAA, a ratio of ≥1.0 proved suitable as cut-off for specific color-coded visualization of the tumor area. Using this method, normal brain was not visualized. The area with the highest pathologic CSI ratios within a given tumor, reflecting the most abnormal metabolite ratio, was defined as CSI_{max} (Cho/Cr_{max} or Cho/NAA_{max}; *figure 1d*).

PET / CSI co-registration (*figure 2*)

Due to lack of spatial information, it is impossible to perform registration of a single slice of CSI metabolic map with an anatomic MR image stack that is routinely used for intraoperative navigation. To enable registration additional anatomic information is needed. Therefore, similarily to Stadlbauer,[30] we performed the following workaround: T2-weighted TSE MR images (15 slices, 2 mm slice thickness) centred around CSI FOV position were obtained. This image stack had FOV identical with CSI FOV (16 x 16 cm) and the matrix resolution identical with the resolution of standard CSI metabolic map (256 x 256). This data set provided the geometrical basis for the data integration into the navigation system. The CSI metabolic maps were projected on five central image slices from this T2-weighted stack, which were interposed between ten empty slices containing only geometric information from the T2-weighted images, five on top and five below the CSI map projections. The central five identical CSI slices of 2 mm thickness represent the real CSI slice acquisition dimension of 1 cm. This MRI/MRS hybrid data set was called “CSI sandwich”.

Prior to surgery, the T2-weighted anatomic dataset was co-registered to the standard T1-weighted contrast-enhanced MR images using the semi-automated registration algorithm of the navigation software (Stealth Station Cranial Mach 5; Medtronic, USA). The system creates a registration matrix file for the T2-weighted anatomic image stack that was manually copied to the folder of the CSI sandwich dataset. This workaround resulted in a co-registration of the T1-weighted anatomic MR image data and the CSI slice.

Topographic correlation of CSI_{max} and PET_{max}

The navigation software provides a rainbow-type color lookup table which converts the grey scale values of the PET and CSI data to a black-red-yellow-green-blue-purple-white color scale[1].

Prior to topographic correlation of CSI_{max} and PET_{max} we used the following windowing adjustments as standard in the navigation system: For removal of background tracer-uptake of normal brain in PET, the *level* slider was set to maximum and the *width* was increased from zero to just before the first background uptake of normal brain appeared. For CSI we used maximum *level* and *width* as standard.

After image fusion with contrast-enhanced MRI, the degree of overlap of CSI_{max} and PET_{max} areas visualized by this method was estimated semiquantitatively by visual impression by two authors (SW, GW) as follows: (1) Cho/Cr_{max} and PET_{max} and, (2) Cho/NAA_{max} and PET_{max}, and (3) Cho/Cr_{max} and Cho/NAA_{max} (*table 1*). The degree of overlap of the maxima of CSI and PET was categorized as follows: (1) overlap ≥ 50%; (2) overlap < 50%; (3) distant (no overlap).

---

[1] Notably, the navigation software color scale is in the opposite direction to the MRI software color scale: CSI_{max} appears in red on the MRI software (see *figures 1* and *5c*) and in white on the navigation software (see *all other figures*).

The center of the CSI and PET areas was regarded as area of maximum metabolism and therefore used as target point for intraoperative tissue sampling with the aid of neuronavigational guidance.

Tissue sampling

Intraoperative navigation was performed with the co-registered CSI/PET/MRI data set. To minimize the effects of potential brain shift in our study, we used either conventional stereotactic biopsy through a burr hole (n=5 of 32 cases, *table 1*) or a technique very similar to a frameless stereotactic biopsy (n=27 of 32 cases): To minimize CSF loss, the patient positioning was selected with the craniotomy at its highest level. Immediately after dural opening, navigation accuracy was verified on surface veins successfully in all patients. Subsequently, the targets inside of CSI_{max} and/or PET_{max} were approached through a small corticotomy using a stereotactic biopsy needle tracked by the navigation system. Sampling of the target area was deliberately performed before tumor resection to ensure a minimal interference with the brain shift that would render the navigation-guided tissue sampling inaccurate.

Intraoperative tissue sampling was performed as follows:

(1) If Cho/Cr_{max} and Cho/NAA_{max} overlap was ≥50%, one tissue sample was taken from this area defined as CSI_{max}.

(2) If Cho/Cr_{max} and Cho/NAA_{max} did not show significant overlap (<50%) specimens were collected from the area of higher metabolite ratio (defined as CSI_{max}).

(3) If CSI_{max} and PET_{max} showed overlap ≥50%, one tissue sample was taken from this area.

(4) If CSI_{max} and PET_{max} showed overlap <50%, separate specimens were taken from both areas.

(5) If PET was negative or showed only unspecific tracer uptake, specimens were taken from CSI_{max}.

To additionally determine the ability of the metabolic imaging methods to detect anaplastic foci, intratumoral tissue samples outside of CSI_{max} and/or PET_{max} were collected as well by using the stereotactic biopsy needle for histopathological correlation purposes. In case of a glioma resection, additionally multiple tissue specimens were collected during tumor removal from intratumoral areas located definitely outside of CSI_{max} and/or PET_{max}, as shown by the navigation system.

Neuropathology

Histopathological tumor typing was performed by the local neuropathology according to the WHO 2007 criteria.[31] In each case, all tumor specimens were systematically analysed by one author (J.A.H) for anaplastic tissue areas (defined as areas with presence of *mitotic figures, necrosis, microvascular proliferation, increased cell density* and *nuclear pleomorphism*) for statistical analysis and to avoid under-grading. For histopathological diagnoses *see table 1*.

Additionally, tumor cell proliferation was assessed immunohistochemically using the *MIB-1* antibody (anti-Ki-67, 1:50; DAKO). MIB-1 binding was apparent as nuclear staining. In each specimen, a total of 500 tumor cell nuclei were evaluated in "hot spots" i.e. fields showing the highest density of Ki-67 immunopositive cells by one author (A.W.), who was unaware of clinical patient characteristics. The fraction of immunolabeled tumor cell nuclei was expressed as percentage (MIB-1 labeling index (LI)).

If more than one sample of CSI_{max}, PET_{max}, and the tumor area outside of CSI_{max} and/or PET_{max} was available, the sample with the most anaplastic histopathologic criteria as described above and with the maximum MIB-1 LI was selected for statistical analysis.

Statistical analysis

For statistical analyses SPSS® version 16.0 software (SPSS Inc., Chicago, Illinois, USA) was used. The presence of histopathologic criteria of anaplasia inside versus outside of CSI_{max} and PET_{max} were compared using the Chi-square test. MIB-1 LI values showed a right-skewed distribution. Thus, for comparison of cell proliferation rates in different areas of a given tumor a non-parametric test (Wilcoxon rank-sum test for paired data) was applied. Values are given as mean and standard deviation. A P-value of <0.05 was considered significant.

RESULTS

Intratumoral metabolite ratios (*table 1*)

CSI ratios were *pathologic* (≥1.0) in all patients: Cho/Cr ratio was 2.7 ± 1.6 (range 1.2 – 9.4), Cho/NAA ratio was 4.4 ± 3.7 (range 1.2 – 14.8).

MET-PET demonstrated *pathologic* (T/N ≥ 1.5) tracer uptake in 21/32 patients: In these cases PET T/N ratio was 2.2 ± 0.7 (range 1.5 – 3.8). However, *normal* (T/N < 1.2) or *non-specific* (T/N 1.2 – 1.4) tracer uptake was encountered in 7 and 4 of 32 patients, respectively.

Topographic correlation

CSI versus PET (*figure 3, table 1*)

Topographic correlation was possible in 21 patients with pathological CSI ratios (ratios ≥1) and unequivocal pathological MET-PET T/N ratios (ratio ≥ 1.5). A ≥50% overlap of CSI (Cho/Cr_{max} and Cho/NAA_{max}) and PET_{max} was found in 18/21 cases and an overlap of <50% was present in 3/21 patients.

Due to the lack of a pathological PET T/N ratio (ratio <1.5), correlation was not possible in 11/32 cases: in 7/11 patients with normal T/N ratio, CSI ratios were pathologic and histopathological examination revealed a glioma WHO grade II in 5 and grade III in 2 patients, respectively. In the remaining 4/11 patients with non-specific tracer uptake, pathological CSI ratios were detected as well (WHO grade II in 2 and grade III in 2 patients, respectively).

CSI: Cho/Cr versus Cho/NAA (*figure 4, table 1*)

An overlap of Cho/Cr_{max} and Cho/NAA_{max} was found ≥50% in 24/32 and <50% in 8/32 cases, respectively. Of the cases with <50% overlap, 6/8 cases exhibited a peculiar pattern with a central Cho/NAA maximum and satellite-like surrounding Cho/Cr maxima.

Histopathologic criteria (*table 2*)

Of the 32 patients with DIG, tissue samples inside and outside of the CSI_{max} and PET_{max} of a given tumor were available in 25 and 17 cases, respectively. In the remaining patients, biopsies were taken only from the site of the metabolic maximum and thus had to be excluded from this analysis.

For the histopathologic criteria of anaplasia (*mitotic figures, necrosis, microvascular proliferation, increased cell density* and *nuclear pleomorphism*), mitotic figures were significantly more frequently present within CSI and PET maxima as compared to peripheral tumor regions. Further, *microvasular proliferation* was significantly more frequently encountered inside PET_{max} and *nuclear pleomorphism* inside CSI_{max} as compared to peripheral tumor areas.

For both CSI and PET, the proliferation rate assessed by MIB-1 LI was significantly higher inside the maximum metabolite ratio area than outside. In the cases with negative or non-specific PET tracer uptake, CSI_{max} still exhibited a significantly higher proliferation rate than in the surrounding tumor areas (10.8% inside CSI_{max} versus 5.2% outside CSI_{max}, *p=0.011*).

DISCUSSION

CSI is a metabolic imaging technique that is widely available and does not expose the patient to radiation exposure. In this study, we investigated the clinical usability of CSI for detection of anaplastic foci in DIG with non-significant CE and performed correlation with MET-PET. We found pathologic CSI ratios in all patients, whereas MET-PET was pathologic in only 21/32 patients. The CSI_{max} and MET-PET_{max} showed significant topographic overlap (≥50%) in the majority of cases (18/21 patients).

Previous studies have shown that MET-PET_{max} represents areas of highest malignancy within DIG.[8,9,11,12] Consequently, we used MET-PET_{max} as reference for topographic correlation with CSI_{max} in our study.

A topographic correlation of the maxima of CSI and PET in DIG has been observed in single cases.[32,33] A systematic topographic analysis has been performed in only two previous small exploratory studies: Go analysed three patients with DIG using multivoxel MRS and L-1-^{11}C-tyrosine-PET.[34] In 2/3 patients the choline MRS and tyrosine PET maxima showed significant topographic correlation, only partial overlap was observed in the third patient.

Stadlbauer reported ≥50% overlap of maxima of CSI (Cho/total NAA) and FET-PET in 11/15 patients and <50% overlap in 4/15 patients.[10] His study design differed from ours by the use of a 1.5 T MRI, FET as PET tracer, inclusion of glioblastomas, biopsy only, the use of Cho/total NAA CSI ratio for topographical correlation with PET only.

Despite of methodological differences, the results of all three CSI-PET correlation studies, including our own study, are similar and indicate that CSI maxima represent metabolically active areas in DIG.

For the detection of metabolically active areas in gliomas by changes in metabolites on MRS, different methods have been described: The calculation of relative metabolite levels in relation to normal brain tissue (such as the Cho-to-NAA index, CNI) has certain advantages, such as the generation of stable measures of Cho abnormality in voxels that have very low or absent NAA.[35] Low or absent levels of NAA, however, are typically encountered in WHO grade IV gliomas which were not the primary pathology of interest in the present study. We therefore assessed the ratios Cho/Cr[18,21-28] and/or Cho/NAA[10,18,21-23,25,26] derived from direct output of the commercially available MRI software package that are most commonly reported in the literature.

Topographic correlation of the maxima of both ratios revealed a high degree of overlap (≥50%) in most cases (24/32 patients). The remaining 8/32 patients showed an overlap of <50%: Six of these

patients (3 oligodendrogliomas, 2 oligoastrocytomas and 1 astrocytoma) had a central Cho/NAA maximum surrounded by multiple satellite-like Cho/Cr maxima. This characteristic pattern has not been described so far. It remains to be shown whether the center and the satellites are histologically different. Future studies could also clarify whether this peculiar Cho/NAA-Cho/Cr pattern is specific to gliomas with oligodendroglioma component, as observed in 5/6 of our cases.

In our series, pathological CSI ratios were detectable even in patients without pathological MET-PET (11/32 cases, *figure 5*). In 4/11 of these patients histological examination revealed an anaplastic glioma. Floeth reported glioma patients with pathologic single voxel spectroscopy but no pathological FET-PET.[5] Nelson reported that MRS was more reliable in tumor identification than ^{18}F-fluorodeoxyglucose-PET in 12/38 cases.[36] These three independent observations indicate that MRS may visualize metabolically active areas within DIG more sensitively than PET.

The number of patients in our series without pathological MET-PET seems high compared to other studies. One possible explanation is the relatively high cutoff value in our series: Whereas other studies used lower cutoffs (between 1.2 and 1.5),[6,7,12,37,38] we defined a rather high cutoff of T/N ratio ≥1.5 as pathologic for the following reasons: According to our experience, gliomas with T/N ratios between 1.15 and <1.5 often demonstrate diffuse tracer uptake without distinct focal maximum. This situation does not allow a reasonable topographic correlation with CSI_{max} as we observed in all 4 patients with T/N ratio between 1.2 and 1.4. In contrast, a distinct focal maximum of MET-PET was detected in all patients with a T/N ratio ≥1.5, which does permit topographic correlation with CSI_{max}.

Cutoff values for pathologic CSI ratios have not been consensually defined in the literature so far. Therefore, we empirically defined CSI ratios of ≥1.0 as pathologic (see *Methods*). Thereby, we achieved specific color-coded visualization of distinct intratumoral CSI maxima, whereas regions in the normal brain were not visualized (*figure 5c*). According to this cutoff definition, all patients in our series had clearly pathologic maxima of CSI.

Herminghaus reported a significant correlation of total choline concentration with MIB-1 LI in neuroepithelial tumors using single voxel MRS, which was proposed as a preoperative tool for tumor grading.[39] Due to potential intratumoral heterogeneity, however, single voxel MRS may miss small anaplastic foci.

To determine the ability of CSI to detect such anaplastic foci, we assessed the WHO criteria of anaplasia as well as the cell proliferation rate measured by MIB-1 LI in tumor samples inside and outside of CSI_{max}: A significantly higher MIB-1 LI, presence of mitotic figures and nuclear pleomorphism was encountered inside the CSI_{max} (*see table 2*). As CSI_{max} and PET_{max} showed significant topographic correlation in the majority of patients, MIB-1 LI, presence of mitotic figures and microvascular proliferation was significantly higher in the area of maximum PET tracer uptake as well. It is of note that even in cases with negative or non-specific PET tracer uptake, CSI was able to depict tumor areas of increased proliferation rate.

Current Limits of CSI

The low spatial resolution of CSI of 1 cm is an inherent limitation for detection of intratumoral anaplastic foci. Compared to the higher resolution of PET (0.4 cm), however, our data demonstrate

that CSI visualization of intumoral "hotspots" correlates with PET_{max} topographically and may be of additional value in cases of negative or non-specific tracer-uptake in PET scan.

The largest diameter of the suspected glioma on T2-weighted images was our key criterion for selection of the single CSI slice, without knowledge of MET-PET findings. Such an approach may miss PET_{max}. Indeed, co-registration of CSI_{max} and PET_{max} revealed a PET_{max} outside of the selected CSI slice in 3/38 patients.

Reliable detection of the metabolically active tumor areas may be achieved by three-dimensional CSI.[35,36] Alternatively, multi-slice CSI could solve the problem. This method uses parallel contiguous CSI slices covering the majority of the tumor volume. We are currently testing the reliability of multi-slice CSI at our center.

Artifacts alter CSI spectra adjacent to bony structures, what impedes reliable detection of superficially localized metabolically active tumor areas. In our patient series, proximity to bone did not allow CSI investigation in the area of PET_{max} in 3/38 patients. CSI software modifications may reduce bone artifacts. However, it seems unlikely that bone artifacts can be completely eliminated. Therefore, PET will remain indispensable for reliable visualization of malignant/metabolically active tumor areas in proximity to the bone.

Outlook

According to our findings, co-registration of CSI with standard anatomic MRI seems to be a promising application that may complement the established PET, functional MRI, and diffusion tensor imaging (DTI) co-registrations and thus optimize multimodal image-guided neurosurgical procedures. Indeed, some other groups also have started to incorporate CSI data into neuronavigation.[30,40]

Conclusion

Our data suggest that CSI using Cho/Cr and Cho/NAA ratios is a clinically reliable non-invasive and widely available technique for detection of anaplastic foci in DIG with non-significant CE. CSI_{max} shows significant topographic correlation with PET_{max} in the majority of our glioma patients. Further, CSI_{max} corresponds to regions with increased proliferative activity within these tumors. Therefore, the intraoperative use of CSI data by multimodal neuronavigation may increase the reliability of detection of malignant areas in DIG with non-significant CE and consequently optimize allocation of patients to adjuvant treatments.

ACKNOWLEDGMENTS

We thank Dr. Harald Heinzl, Department of Medical Computer Sciences, for statistical advice, Brigitte Dobsak for drawing the illustration and Irene Leisser& Gerda Ricken for technical assistance with preparation of tissue specimens.

Competing Interest: None declared

Funding: None declared

REFERENCE LIST

1. Barker FG, 2nd, Chang SM, Huhn SL, Davis RL, Gutin PH, McDermott MW, et al. Age and the risk of anaplasia in magnetic resonance-nonenhancing supratentorial cerebral tumors. *Cancer* 1997;80(5):936-41.
2. Ginsberg LE, Fuller GN, Hashmi M, Leeds NE, Schomer DF. The significance of lack of MR contrast enhancement of supratentorial brain tumors in adults: histopathological evaluation of a series. *Surg.Neurol.* 1998;49(4):436-440.
3. Kondziolka D, Lunsford LD, Martinez AJ. Unreliability of contemporary neurodiagnostic imaging in evaluating suspected adult supratentorial (low-grade) astrocytoma. *J.Neurosurg.* 1993;79(4):533-536.
4. Pallud J, Capelle L, Taillandier L, Fontaine D, Mandonnet E, Guillevin R, et al. Prognostic Significance of Imaging Contrast Enhancement for WHO grade II Gliomas. *Neuro.Oncol.* 2008.
5. Floeth FW, Pauleit D, Wittsack HJ, Langen KJ, Reifenberger G, Hamacher K, et al. Multimodal metabolic imaging of cerebral gliomas: positron emission tomography with [18F]fluoroethyl-L-tyrosine and magnetic resonance spectroscopy. *J.Neurosurg.* 2005;102(2):318-327.
6. Gumprecht H, Grosu AL, Souvatsoglou M, Dzewas B, Weber WA, Lumenta CB. 11C-Methionine positron emission tomography for preoperative evaluation of suggestive low-grade gliomas. *Zentralbl.Neurochir.* 2007;68(1):19-23.
7. Hatakeyama T, Kawai N, Nishiyama Y, Yamamoto Y, Sasakawa Y, Ichikawa T, et al. (11)C-methionine (MET) and (18)F-fluorothymidine (FLT) PET in patients with newly diagnosed glioma. *Eur.J.Nucl.Med.Mol.Imaging* 2008.
8. Roessler K, Gatterbauer B, Becherer A, Paul M, Kletter K, Prayer D, et al. Surgical target selection in cerebral glioma surgery: linking methionine (MET) PET image fusion and neuronavigation. *Minim.Invasive.Neurosurg.* 2007;50(5):273-280.
9. Singhal T, Narayanan TK, Jain V, Mukherjee J, Mantil J. 11C-L-methionine positron emission tomography in the clinical management of cerebral gliomas. *Mol.Imaging Biol.* 2008;10(1):1-18.
10. Stadlbauer A, Prante O, Nimsky C, Salomonowitz E, Buchfelder M, Kuwert T, et al. Metabolic imaging of cerebral gliomas: spatial correlation of changes in O-(2-18F-fluoroethyl)-L-tyrosine PET and proton magnetic resonance spectroscopic imaging. *J.Nucl.Med.* 2008;49(5):721-729.
11. Goldman S, Levivier M, Pirotte B, Brucher JM, Wikler D, Damhaut P, et al. Regional methionine and glucose uptake in high-grade gliomas: a comparative study on PET-guided stereotactic biopsy. *J.Nucl.Med.* 1997;38(9):1459-1462.
12. Sadeghi N, Salmon I, Decaestecker C, Levivier M, Metens T, Wikler D, et al. Stereotactic comparison among cerebral blood volume, methionine uptake, and histopathology in brain glioma. *AJNR Am.J.Neuroradiol.* 2007;28(3):455-461.
13. Pirotte B, Goldman S, Dewitte O, Massager N, Wikler D, Lefranc F, et al. Integrated positron emission tomography and magnetic resonance imaging-guided resection of brain tumors: a report of 103 consecutive procedures. *J Neurosurg* 2006;104(2):238-53.

14. Tanaka Y, Nariai T, Momose T, Aoyagi M, Maehara T, Tomori T, et al. Glioma surgery using a multimodal navigation system with integrated metabolic images. *J Neurosurg* 2009;110(1):163-72.
15. Ceyssens S, Van LK, de GT, Goffin J, Bormans G, Mortelmans L. [11C]methionine PET, histopathology, and survival in primary brain tumors and recurrence. *AJNR Am.J.Neuroradiol.* 2006;27(7):1432-1437.
16. Hattingen E, Raab P, Franz K, Lanfermann H, Setzer M, Gerlach R, et al. Prognostic value of choline and creatine in WHO grade II gliomas. *Neuroradiology* 2008.
17. Isobe T, Matsumura A, Anno I, Yoshizawa T, Nagatomo Y, Itai Y, et al. Quantification of cerebral metabolites in glioma patients with proton MR spectroscopy using T2 relaxation time correction. *Magn Reson.Imaging* 2002;20(4):343-349.
18. Negendank WG, Sauter R, Brown TR, Evelhoch JL, Falini A, Gotsis ED, et al. Proton magnetic resonance spectroscopy in patients with glial tumors: a multicenter study. *J.Neurosurg.* 1996;84(3):449-458.
19. Sibtain NA, Howe FA, Saunders DE. The clinical value of proton magnetic resonance spectroscopy in adult brain tumours. *Clin.Radiol.* 2007;62(2):109-119.
20. Stadlbauer A, Gruber S, Nimsky C, Fahlbusch R, Hammen T, Buslei R, et al. Preoperative grading of gliomas by using metabolite quantification with high-spatial-resolution proton MR spectroscopic imaging. *Radiology* 2006;238(3):958-969.
21. Croteau D, Scarpace L, Hearshen D, Gutierrez J, Fisher JL, Rock JP, et al. Correlation between magnetic resonance spectroscopy imaging and image-guided biopsies: semiquantitative and qualitative histopathological analyses of patients with untreated glioma. *Neurosurgery* 2001;49(4):823-829.
22. Fayed N, Morales H, Modrego PJ, Pina MA. Contrast/Noise ratio on conventional MRI and choline/creatine ratio on proton MRI spectroscopy accurately discriminate low-grade from high-grade cerebral gliomas. *Acad.Radiol.* 2006;13(6):728-737.
23. Guillevin R, Menuel C, Duffau H, Kujas M, Capelle L, Aubert A, et al. Proton magnetic resonance spectroscopy predicts proliferative activity in diffuse low-grade gliomas. *J.Neurooncol* 2008;87(2):181-187.
24. Jeun SS, Kim MC, Kim BS, Lee JM, Chung ST, Oh CH, et al. Assessment of malignancy in gliomas by 3T 1H MR spectroscopy. *Clin.Imaging* 2005;29(1):10-15.
25. Law M, Yang S, Wang H, Babb JS, Johnson G, Cha S, et al. Glioma grading: sensitivity, specificity, and predictive values of perfusion MR imaging and proton MR spectroscopic imaging compared with conventional MR imaging. *AJNR Am.J.Neuroradiol.* 2003;24(10):1989-1998.
26. Shimizu H, Kumabe T, Tominaga T, Kayama T, Hara K, Ono Y, et al. Noninvasive evaluation of malignancy of brain tumors with proton MR spectroscopy. *AJNR Am.J.Neuroradiol.* 1996;17(4):737-747.
27. Tamiya T, Kinoshita K, Ono Y, Matsumoto K, Furuta T, Ohmoto T. Proton magnetic resonance spectroscopy reflects cellular proliferative activity in astrocytomas. *Neuroradiology* 2000;42(5):333-338.
28. Toyooka M, Kimura H, Uematsu H, Kawamura Y, Takeuchi H, Itoh H. Tissue characterization of glioma by proton magnetic resonance spectroscopy and perfusion-weighted magnetic resonance imaging: glioma grading and histological correlation. *Clin.Imaging* 2008;32(4):251-258.

29. Potzi C, Becherer A, Marosi C, Karanikas G, Szabo M, Dudczak R, et al. [11C] methionine and [18F] fluorodeoxyglucose PET in the follow-up of glioblastoma multiforme. *J Neurooncol* 2007;84(3):305-14.
30. Stadlbauer A, Moser E, Gruber S, Nimsky C, Fahlbusch R, Ganslandt O. Integration of biochemical images of a tumor into frameless stereotaxy achieved using a magnetic resonance imaging/magnetic resonance spectroscopy hybrid data set. *J.Neurosurg.* 2004;101(2):287-294.
31. Louis DN, Ohgaki H, Wiestler OD, Cavenee WK. *WHO Classifcation of tumours of the central nervous system. IARC, Lyon*, 2007.
32. Go KG, Keuter EJ, Kamman RL, Pruim J, Metzemaekers JD, Staal MJ, et al. Contribution of magnetic resonance spectroscopic imaging and L-[1-11C]tyrosine positron emission tomography to localization of cerebral gliomas for biopsy. *Neurosurgery* 1994;34(6):994-1002.
33. Luyten PR, Marien AJ, Heindel W, van Gerwen PH, Herholz K, den Hollander JA, et al. Metabolic imaging of patients with intracranial tumors: H-1 MR spectroscopic imaging and PET. *Radiology* 1990;176(3):791-799.
34. Go KG, Kamman RL, Mooyaart EL, Heesters MA, Pruim J, Vaalburg W, et al. Localised proton spectroscopy and spectroscopic imaging in cerebral gliomas, with comparison to positron emission tomography. *Neuroradiology* 1995;37(3):198-206.
35. McKnight TR, Lamborn KR, Love TD, Berger MS, Chang S, Dillon WP, et al. Correlation of magnetic resonance spectroscopic and growth characteristics within Grades II and III gliomas. *J.Neurosurg.* 2007;106(4):660-666.
36. Nelson SJ, Vigneron DB, Dillon WP. Serial evaluation of patients with brain tumors using volume MRI and 3D 1H MRSI. *NMR Biomed.* 1999;12(3):123-138.
37. Herholz K, Holzer T, Bauer B, Schroder R, Voges J, Ernestus RI, et al. 11C-methionine PET for differential diagnosis of low-grade gliomas. *Neurology* 1998;50(5):1316-1322.
38. Kracht LW, Miletic H, Busch S, Jacobs AH, Voges J, Hoevels M, et al. Delineation of brain tumor extent with [11C]L-methionine positron emission tomography: local comparison with stereotactic histopathology. *Clin.Cancer Res.* 2004;10(21):7163-7170.
39. Herminghaus S, Pilatus U, Moller-Hartmann W, Raab P, Lanfermann H, Schlote W, et al. Increased choline levels coincide with enhanced proliferative activity of human neuroepithelial brain tumors. *NMR Biomed* 2002;15(6):385-92.
40. Son BC, Kim MC, Choi BG, Kim EN, Baik HM, Choe BY, et al. Proton magnetic resonance chemical shift imaging (1H CSI)-directed stereotactic biopsy. *Acta Neurochir.(Wien.)* 2001;143(1):45-49.

Table 1- Patient Characteristics

case	age	sex	extent of surgery	repeat surgery	localization	side	diagnosis	WHO grade	PET	CSI		Correlation of Maxima		
									T/N ratio	Cho/Cr ratio	Cho/NAA ratio	PET vs CSI (Cho/Cr)	PET vs CSI (Cho/NAA)	CSI (Cho/Cr) vs CSI (Cho/NAA)
1	37	m	GTR	no	central	right	astrocytoma	2	1.1	1.2	1.5	PET neg	PET neg	++
2	48	f	PR	yes	frontal	right	astrocytoma	2	1.5	1.9	2.6	++	++	++
3	38	m	GTR	no	frontal	left	astrocytoma	2	1.0	1.9	1.6	PET neg	PET neg	++
4	44	m	PR	no	insular	left	astrocytoma	2	1.0	1.7	6.2	PET neg	PET neg	+ [1]
5	44	f	B	yes	insular	right	astrocytoma	2	2.0	2.7	5.9	++	++	++
6	32	f	GTR	no	central	left	astrocytoma	3	1.3	2.0	3.2	PET non spec	PET non spec	++
7	50	m	PR	no	temporal	left	astrocytoma	3	2.6	1.5	5.0	++	++	++
8	47	f	GTR	no	insular	right	astrocytoma	3	2.6	4.4	5.7	++	++	++
9	34	f	GTR	yes	insular	right	astrocytoma	3	1.7	2.1	1.8	++	++	++
10	29	m	GTR	no	frontal	left	astrocytoma	3	1.7	3.5	13.0	+	+	++
11	25	f	B	yes	occipital	left	astrocytoma	3	1.7	3.0	14.7	++	++	++
12	26	m	GTR	no	central	right	astrocytoma	3	0.9	2.7	4.9	PET neg	PET neg	++
13	65	f	GTR	no	frontal	right	mixed oligoastrocytoma	2	1.3	1.2	1.3	PET non spec	PET non spec	+
14	44	f	GTR	no	temporal	left	mixed oligoastrocytoma	2	1.0	1.6	1.6	PET neg	PET neg	++
15	46	f	GTR	no	frontal	left	mixed oligoastrocytoma	2	1.0	1.7	1.3	PET neg	PET neg	++
16	34	f	GTR	no	frontal	left	mixed oligoastrocytoma	3	1.2	1.7	2.2	PET non spec	PET non spec	++
17	23	m	GTR	no	frontal	right	mixed oligoastrocytoma	3	2.2	2.8	2.8	++	++	+
18	54	m	GTR	yes	insular	right	mixed oligoastrocytoma	3	2.3	6.3	2.9	+	+	++
19	66	m	GTR	no	insular	right	mixed oligoastrocytoma	3	1.6	3.0	8.3	++	++	+ [1]
20	59	m	B	yes	insular	left	mixed oligoastrocytoma	3	2.6	9.4	13.1	++	++	+ [1]
21	46	f	GTR	no	insular	right	oligodendroglioma	2	1.4	1.7	1.7	PET non spec	PET non spec	++
22	43	m	PR	yes	parietal	left	oligodendroglioma	2	2.4	2.3	1.9	++	++	++
23	48	m	PR	no	temporal	right	oligodendroglioma	2	1.5	2.0	1.2	+	+	+ [1]
24	40	f	B	no	temporal	left	oligodendroglioma	2	1.5	2.7	4.8	++	++	++
25	25	f	GTR	no	central	left	oligodendroglioma	2	3.0	1.6	1.8	++	++	++
26	16	m	GTR	no	frontal	left	oligodendroglioma	3	1.1	2.4	2.9	PET neg	PET neg	++
27	27	f	GTR	no	temporal	left	oligodendroglioma	3	3.3	2.2	11.1	++	++	++
28	63	f	GTR	no	central	left	oligodendroglioma	3	1.6	2.8	2.4	++	++	+ [1]
29	48	m	GTR	no	occipital	right	oligodendroglioma	3	1.6	3.8	4.6	++	++	++
30	48	m	GTR	no	frontal	left	oligodendroglioma	3	1.6	2.3	2.1	++	++	++
31	27	f	PR	yes	frontal	right	oligodendroglioma	3	3.9	2.3	2.3	++	++	+ [1]
32	42	m	B	yes	frontal	right	oligodendroglioma	3	2.0	2.7	3.9	++	++	++

GTR...gross total resection; PR...partial resection; B...biopsy

Cho...choline; Cr...creatine; NAA...N-acetyl aspartat; T/N ratio...tumor/normal ratio

++...overlap ≥ 50%; +...overlap < 50%;PET non spec...non specific tracer uptake;PET neg...no tracer uptake

[1] central Cho/NAA maximum, peripheral Cho/Cr maxima

Table 2- Histopathologic Criteria

	n	*MIB-1 LI*		*Mitosis*		*Necrosis*		*Microvascular proliferation*		*Cell density*		*Nuclear pleomorphism*	
		mean ± SD	*p*	*present*	*p*	*present*	*p*	*present*	*p*	*high*	*p*	*present*	*p*
CSI	25												
inside CSImax		13.6 ± 11.4	**< 0.001**	14 (82%)	**0.002**	1 (100%)	n.s.	5 (83%)	n.s.	20 (59%)	n.s.	20 (67%)	**0.009**
outside CSImax		6.9 ± 4.5		3 (18%)		0 (0%)		1 (17%)		14 (41%)		10 (33%)	
PET	17												
inside PETmax		14.9 ± 11.7	**0.004**	19 (77%)	**0.001**	1 (100%)	n.s.	6 (86%)	**0.009**	14 (50%)	n.s.	12 (55%)	n.s.
outside PETmax		7.8 ± 4.8		3 (23%)		0 (0%)		1 (14%)		14 (50%)		10 (45%)	
subgroup overlap PETmax and CSImax <50%	3												
inside CSImax		7.1 ± 4.2	n.s.	2 (67%)	n.s.	0 (0%)	-	0 (0%)	n.s.	4 (50%)	n.s.	4 (57%)	n.s.
inside PETmax		5.3 ± 0.7		1 (33%)		0 (0%)		1 (100%)		4 (50%)		3 (43%)	
subgroup PET neg/non spec and CSI pathological	9												
inside CSImax		10.8 ± 11.4	**0.011**	3 (100%)	n.s.	0 (0%)	-	0 (0%)	-	6 (55%)	n.s.	7 (78%)	n.s.
outside CSImax		5.2 ± 3.6		0 (0%)		0 (0%)		0 (0%)		5 (45%)		2 (22%)	

PET non spec...non specific tracer uptake; PET neg...no tracer uptake

LEGENDS TO FIGURES

Figure 1 – Methods - CSI data processing and metabolic ratio map creation.

(a) Matrix (8x10) of multivoxel ^{1}H magnetic-resonance-spectra from fronto-parietal brain region including the tumor lesion.

(b) Maps of the metabolic ratios Cho/NAA are produced using the spectroscopy application within the spectrometer operating system. After zero filling, phasing, filtering of the data, polynomial baseline correction was applied and line fit in the frequency domain was used to obtain Cho and NAA signal intensity.

(c) Metabolic ratio maps were created within the VOI using the numerical value interpolation as implemented by the manufacturer. Lower limit of the color map (blue) corresponds to a value of Cho/NAA 0.39 in this patient.

(d) Rescaling of color map according to the predefined pathologic CSI ratio of ≥1: The blue color code now corresponds to the CSI_{min} of 1.00. The red color code visualizes the tumor area with the highest Cho/NAA CSI ratio (CSI_{max} = 1.96 in this patient).

Figure 2 – Methods - Registration of single-slice CSI on morphologic MRI data for intraoperative navigation:

Step 1 – Image registration of T2-weighted anatomic dataset (co-planar to CSI stack) to the standard T1-weighted contrast-enhanced MR images.

Step 2 – Manual copying of the resulting registration matrix file from the T2-weighted anatomic image stack to the folder of the CSI sandwich dataset on the navigation system.

Step 3 – For intraoperative application, the resulting registered morphologic T1-weighted and metabolic CSI image datasets are loaded into the navigation system.

Figure 3 – Topographic correlation of MET-PET and CSI maxima:

a – c: Right parietal oligodendroglioma WHO grade III (*case 22*). a: PET_{max}, b: CSI Cho/Cr_{max}, c: PET/CSI co-registration resulting in >50% maxima overlap.

d – f: Left precentral oligodendroglioma WHO grade II (*case 25*). d: PET_{max}, e: CSI Cho/NAA_{max}, f: PET/CSI co-registration resulting in <50% maxima overlap.

Figure 4 – Topographic correlation of CSI Cho/Cr and CSI Cho/NAA maxima:

a – c: Left frontal oligodendroglioma WHO grade III (*case 30*). a: Cho/NAA_{max}, b: Cho/Cr_{max}, c: Cho/NAA and Cho/Cr co-registration resulting in >50% maxima overlap.

d – f: Right insular oligoastrocytoma WHO grade III (*case 19*). d: Cho/NAA_{max}, e: Cho/Cr_{max}, f: Cho/NAA and Cho/Cr co-registration resulting in <50% maxima overlap. Note the central Cho/NAA maximum and satellite-like surrounding Cho/Cr maxima.

Figure 5 – Non-specific MET-PET tracer uptake with CSI_{max} in a left precentral oligoastrocytoma WHO grade III (*case 16*):

a: T1-weighted contrast-enhanced MRI: Note the non-enhancing left precentral lesion, b: MET-PET without distinct focal maximum, c: Complete single-slice CSI (Cho/NAA) as derived from MR post-

processing depicts a central CSI_{max}. d: Focused CSI_{max} (Cho/NAA) after windowing at the navigation workstation. e – f: Tissue sample from CSI_{max}. e: HE depicts prominent anaplasia of the astrocytic tumor part with brisk mitotic activity (*magnification x200*). f: MIB-1 labeling index of the Ki-67 antigen > 40% (*magnification x400*). g-h: Tissue sample from outside of CSI_{max}. g: HE depicts a low-grade tumor area; h: MIB-1 labeling index of the Ki-67 antigen <9%.

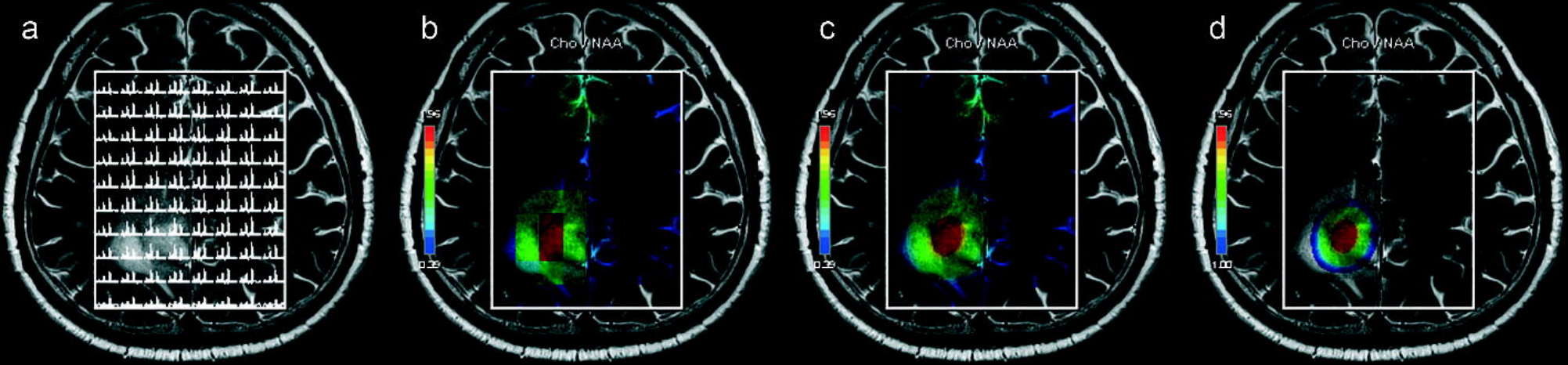
a
b
Cho/NAA
1.95
0.39
c
Cho/NAA
1.95
0.39
d
Cho/NAA
1.95
1.00

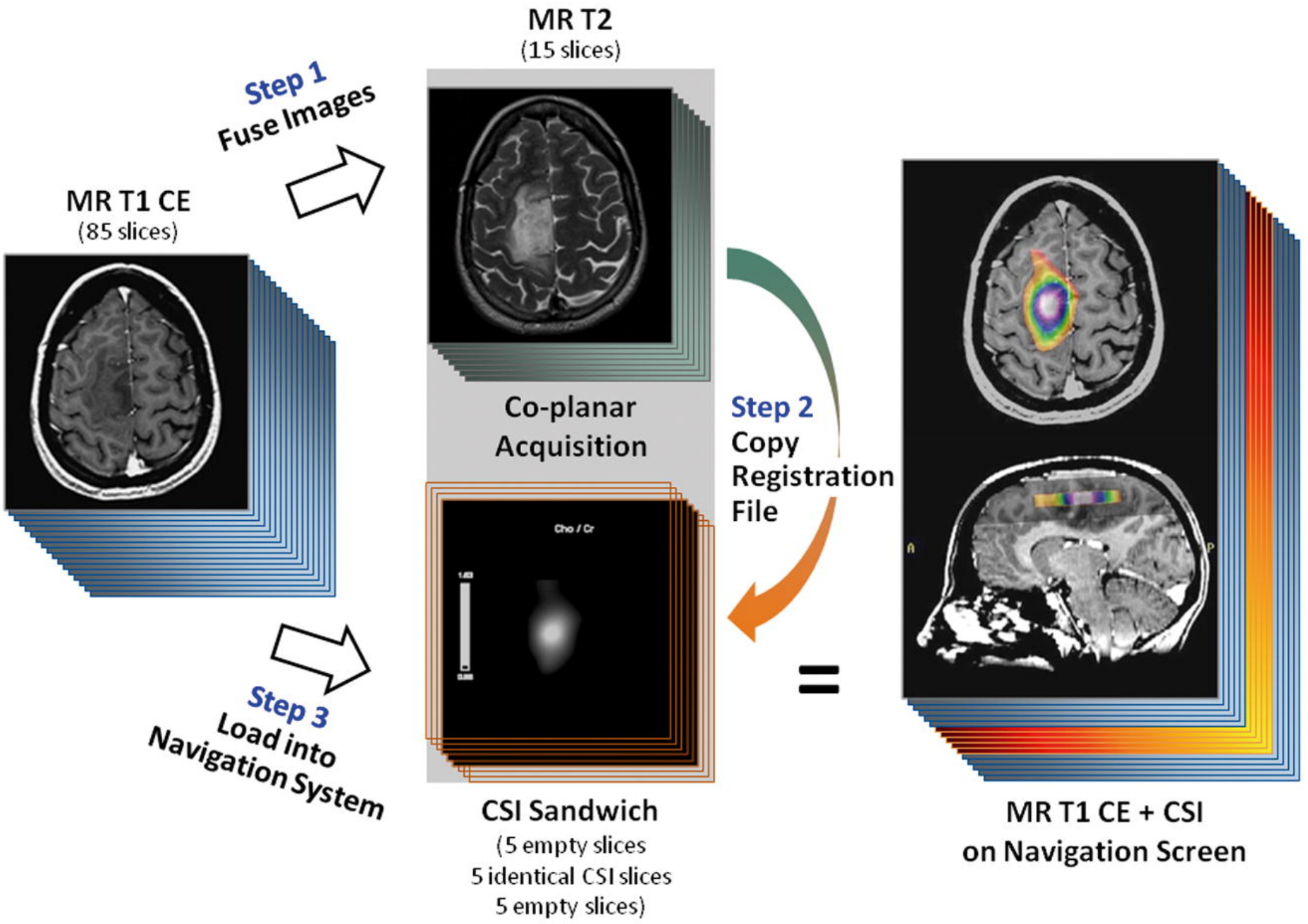
MR T2
(15 slices)
Step 1
Fuse Images
MR T1 CE
(85 slices)
Co-planar
Acquisition
Step 2
Copy
Registration
File
Cho / Cr
Step 3
Load into
Navigation System
=
CSI Sandwich
(5 empty slices
5 identical CSI slices
5 empty slices)
MR T1 CE + CSI
on Navigation Screen

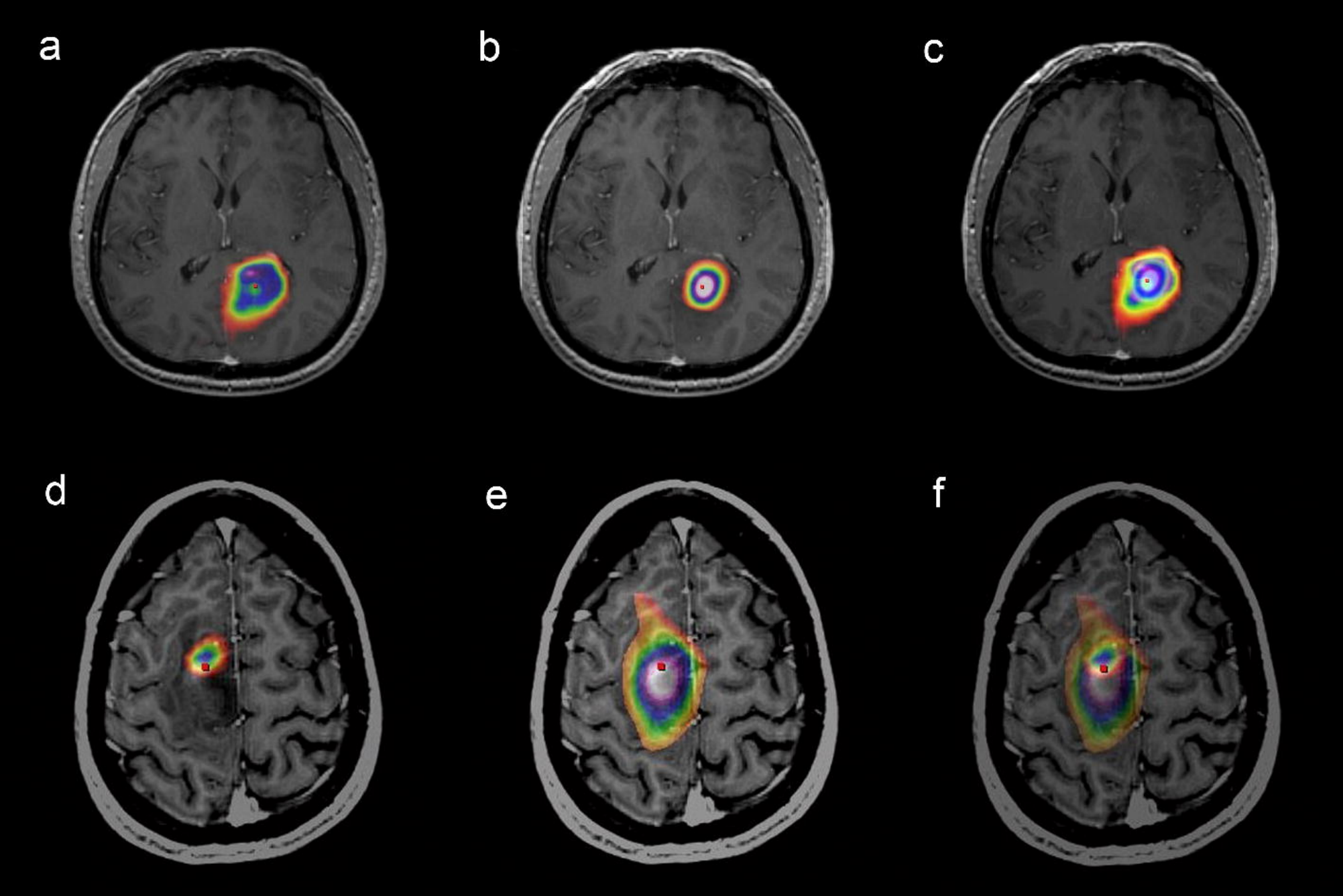
a
b
c
d
e
f

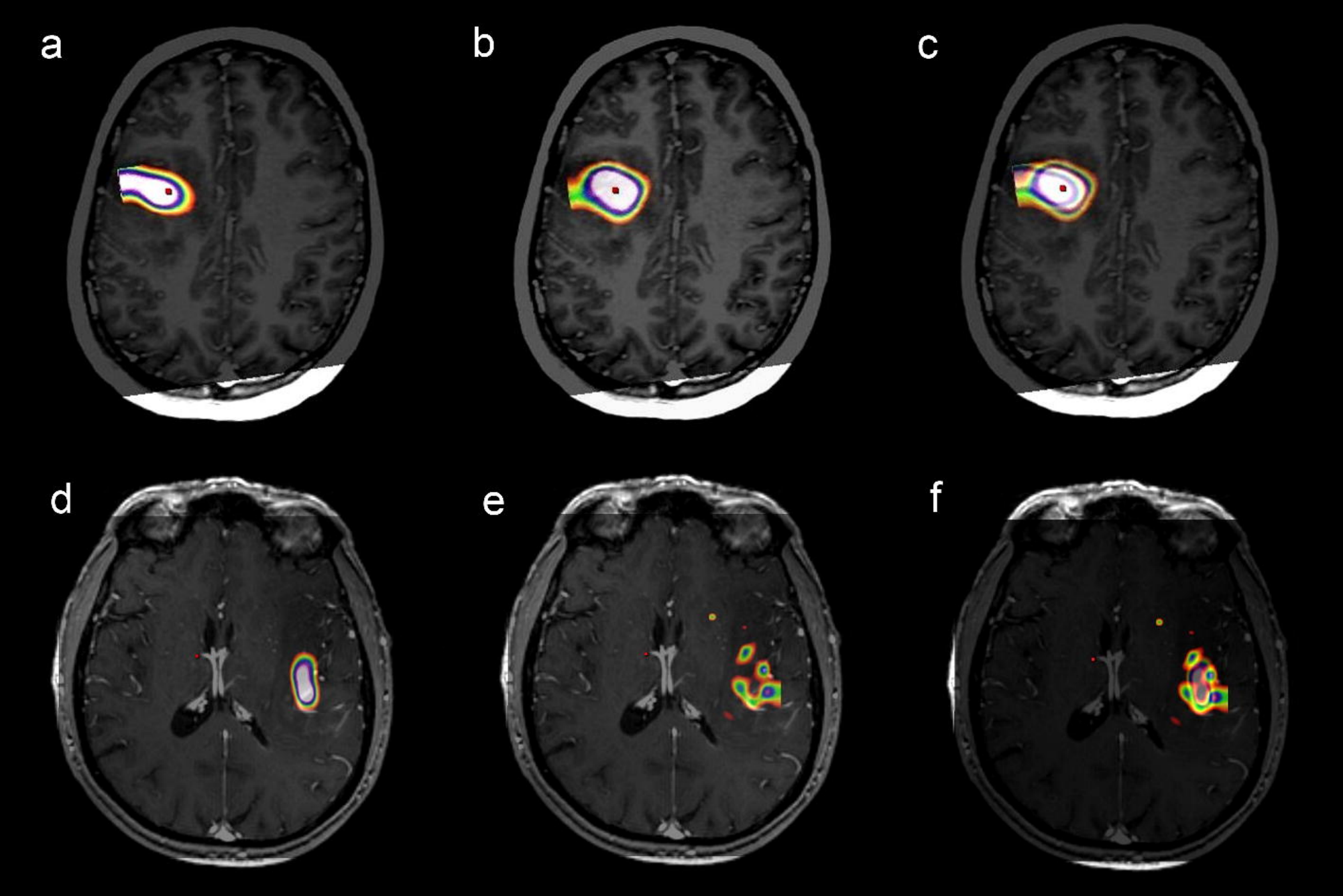
a
b
c
d
e
f

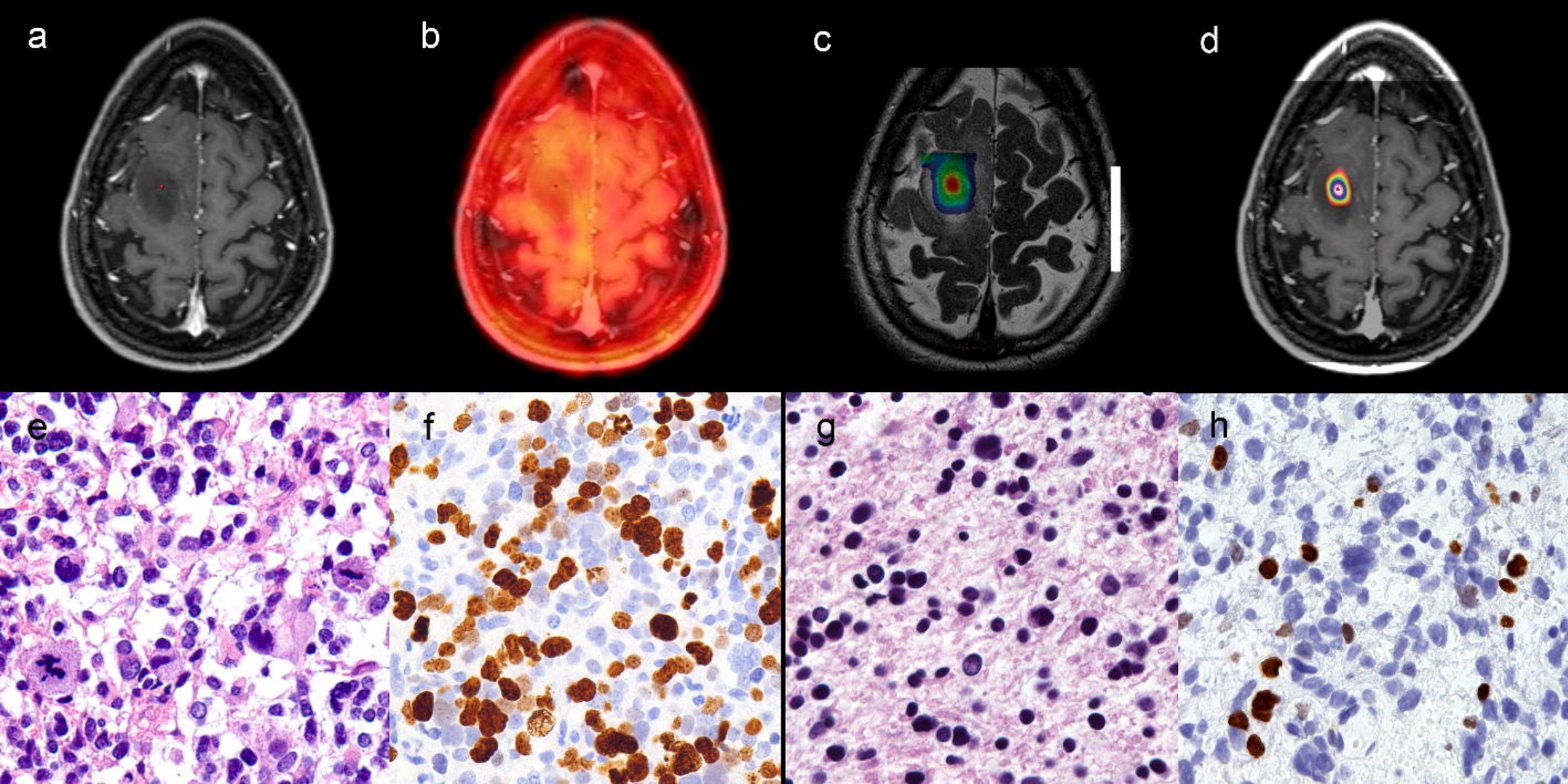
a
b
c
d
e
f
g
h